

Rashba-driven anomalous Nernst conductivity of lead chalcogenide films

Parijat Sengupta¹ and Junxia Shi¹

Dept. of Electrical Engineering, University of Illinois, Chicago, IL 60607.

The presence of a finite Berry curvature ($\Omega(k)$) leads to anomalous thermal effects. In this letter, we compute the coefficients for the anomalous Nernst effect (*ANE*) and its spin analogue, the spin Nernst effect (*SNE*) in lead chalcogenide (PbX ; $X = \text{S, Se, Te}$) films. The narrow gapped PbX films with a large spin-orbit coupling (*soc*) offer a significant Rashba interaction that gives rise to $\Omega(k)$ and the attendant anomalous thermal behaviour. In presence of a temperature gradient, the *ANE* and *SNE* establish a thermal and spin current and are characterized by their respective coefficients which acquire higher values for a stronger Rashba interaction. We further show that an extrinsic *soc* generated by an in-plane electric field offers a gate-like mechanism to control (and turn-off) the anomalous thermal currents. Finally, we conclude by deriving the efficiency of an *ANE*-driven low-temperature Carnot heat engine and demonstrate that it can be gainfully optimized in systems with a robust intrinsic *soc* resulting in low carrier effective masses.

The Nernst effect (*NE*) describes the generation of a transverse electric field by a longitudinal temperature gradient in presence of an out-of-plane magnetic field. The related Nernst coefficient is nominally expressed as $\mathcal{N} = E_y / (-\nabla T_x)$.¹ The Nernst-induced electric field and the temperature gradient exist along the y - and x -axes, respectively. A variant of *NE* in absence of a real-space magnetic field has also been observed²; the magnetic field, instead, is supplied by an analogous quantity - the Berry curvature.³ The Berry curvature ($\Omega(k)$) as an effective magnetic field in momentum space (k) imparts a Lorentz force on carrier electrons giving rise to an ‘anomalous’ velocity that is the precursor to a variety of observed effects, an illustration of which is the anomalous Nernst effect (*ANE*). The *ANE* has been theoretically predicted in a wide selection of materials including the d -density wave state in cuprate superconductors⁴, illuminated graphene⁵, and monolayer group-VI dichalcogenides.⁶ In each of these family of materials, it is possible to write a prototypical Hamiltonian transformable along a closed contour in momentum space in a cyclic adiabatic process giving rise to the non-zero Berry connection ($\mathcal{A}(k)$) from which an equivalent magnetic field ($\Omega(k) = \nabla_k \times \mathcal{A}(k)$) can be defined. For the case of graphene-like materials and the dichalcogenides, in the presence of either broken inversion or time-reversal symmetry (*TRS*), the form of Hamiltonian that sets up a finite $\Omega(k)$ is of a massive Dirac-type: $\mathcal{H}_{eff} = \nu(\sigma_x k_y - \sigma_y k_x) + \Delta \sigma_z$. The constant ν has units of $eV \text{\AA}$ and Δ is the generalized Dirac mass. The Pauli matrices (σ_i) may act on the lattice or spin sub-space.

It is easy to note, however, that the form of the k -dependent part of the Hamiltonian that permits a finite $\Omega(k)$ also describes the linear Rashba spin-orbit coupling (*RSOC*) for Bloch conduction electrons.⁷ For a set of conduction electrons in a thin film (quantum well) that follow a quadratic dispersion and split into the linear *RSOC*-induced spin-polarized sub-bands, it is reasonable to anticipate the occurrence of a similarly definable $\Omega(k)$. The $\Omega(k)$ in this case would be solely an outcome of the linear *RSOC* Hamiltonian; the quadratic term does not contribute. A non-vanishing $\Omega(k)$ therefore alludes to the appearance of a concomitant *ANE*,

the analytic estimation of which is the chief purpose here. We quantitatively estimate the strength of *ANE* in thin films whose Bloch conduction bands are split by *RSOC* in spin-polarized ensembles and examine underlying dependencies that enhance this thermomagnetic process. An additional purported aim is also to uncover avenues that potentially optimize the efficiency of *ANE* via changes to strength of *RSOC*, the band curvature (tied to film dimensions), and external impurities. In fact, since an avowed goal in recent times hinges on the design of ‘energy-harvesting’ techniques, a large *ANE* can complement the *NE* in miniaturized magneto-thermal devices.

It is worthwhile though to clarify that while a definite $\Omega(k)$ is derivable from a *RSOC* Hamiltonian and assumes an identical form to that obtained for gapped graphene-like materials and chalcogenides⁸, the genesis of it lies in the spin degree of freedom unlike an inversion breaking mixing of orbitals in the latter. This disparity in the origin of the emergence of $\Omega(k)$ aside, it is significant to observe that *RSOC* is only operational when inversion symmetry is lost, which essentially constitutes one of the prerequisites (the other is *TRS* and at least one must be satisfied) for a non-vanishing $\Omega(k)$ and fulfilled by the graphene family and dichalcogenides. Evidently, for a discernible $\Omega(k)$ (and *ANE*), a primary requirement centers around a large *RSOC*, a quantity generally pronounced in confined structures of compounds with narrow band gaps and high intrinsic spin-orbit coupling. While several sets of materials display a robust *RSOC*, it is beneficial to recall the thermal basis of the parent *NE* and thus select a candidate system that also combines favourable thermoelectric behaviour. The lead chalcogenides⁹ - PbX ($X = \text{S/Se/Te}$) - conform well in this regard, possessing the necessary material attributes for a large *RSOC* and a high thermoelectric figure of merit (ZT). PbTe and its alloyed derivatives have been widely researched for achieving an enhanced ZT .¹⁰

In an n -doped PbTe sample under an out-of-plane magnetic field (causing a Zeeman split) and a temperature gradient (Fig. 1), we show that the *ANE* responds to a Rashba-controlled Berry curvature distribution in momentum space and can be further modulated with an in-plane electric field. A complete cessation of *ANE* (van-

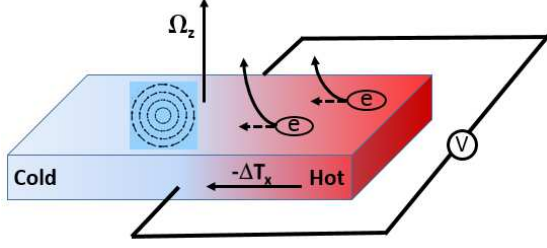


FIG. 1. A schematic depiction of the anomalous Nernst effect in a PbTe (representative PbX) slab with a temperature gradient along the x -axis. The Rashba coupled Bloch conduction electrons with the characteristic helical in-plane spin polarization shown on the slab surface generates $\Omega(k)$, a momentum-dependent magnetic field along the z -axis (out-of-plane). An external z -axis aligned magnetic field (not shown) is also applied to the PbTe slab. An anomalous voltage develops in a direction transverse (y -axis) to $\nabla_x T$.

ishing $\Omega(k)$ happens when the in-plane electric field initiated spin-orbit coupling (*soc*) exactly annuls the Zeeman splitting. An accompanying quantifiable spin current - the anomalous spin Nernst effect - also flows mirroring the pattern observed for *ANE*. In the last part, we develop the idea of an *ANE*- driven Carnot engine whose efficiency is shown to be optimized by low carrier effective masses - the hallmark of high *soc* that also greatly influences *RSOC*.

For an analytic formulation, we begin by writing the expression for *ANE* which is $J_y = \mathcal{N}'(-\nabla_x T)$. The primed coefficient \mathcal{N}' distinguishes from \mathcal{N} , the corresponding notation for *NE*. The *ANE* coefficient is¹¹

$$\mathcal{N}' = \frac{ek_B}{\hbar} \sum_{\pm} \int \frac{d^2\mathbf{k}}{4\pi^2} \Omega(k) \mathcal{S}(k). \quad (1)$$

where $\mathcal{S}(k)$ is the entropy density. The entropy density is defined as: $\mathcal{S}(k) = -f_k \ln f_k - (1-f_k) \ln(1-f_k)$. Here f_k is the usual Fermi distribution function. The summation over the spin-split bands is indicated by \pm under the \sum operator. As a brief insight into the particular form of the *ANE* coefficient (Eq. 1), we simply note that a finite $\Omega(k)$ lets the electron carriers (of charge ' e ' and in presence of an electric field \mathbf{E}) acquire an additional velocity $v_{ane} = (e\mathbf{E}/\hbar) \times \Omega(k)$. Multiplying v_{ane} by the entropy density furnishes the coefficient for the transverse heat current from which we obtain \mathcal{N}' in Eq. 1. The primary task, therefore, to proceed further with *ANE* calculations is a determination of $\Omega(k)$. To do so, we first write down the minimal Hamiltonian that describes the Rashba and Zeeman spin-split parabolic conduction bands in a PbX quantum well. It is simply given by

$$H_0 = \frac{p^2}{2m^*} + \alpha_R (\sigma_x k_y - \sigma_y k_x) + \Delta \sigma_z. \quad (2)$$

The Pauli matrices in Eq. 2 act on the spin-space and the parameter Δ is the the out-of-plane magnetic field governed Zeeman splitting. The Rashba coupling pa-

rameter is α_R with adjustable strength via a gate electrode while the effective mass is m^* , which here are for the L -valley conduction electrons of a PbX film (quantum well confined along the z -axis). The corresponding eigen states are $\varepsilon_{\pm} = p^2/2m^* \pm \alpha_R k \pm \Delta$. The upper (lower) sign is for the spin-up (down) band. Additionally, we consider only conduction electrons (*CE*) of the PbX film (rock salt crystal structure) that belong to the L -valley and whose axis coincides with the $[111]$ direction. Note that there exist three other oblique valleys with axes mis-aligned to the $[111]$ vector.¹⁴ We make use of a 4×4 $k.p$ Hamiltonian^{12,13} that captures the dispersion around the high-symmetry L -valley; substituting for the confined $k_z = -i\partial_z$ in the Hamiltonian and followed by a numerical diagonalization supplies the quantum well *CE* effective mass.¹⁴ The presented calculations use PbTe as the representative PbX .

For a quantum well, which is a two-dimensional system whose Hamiltonian (disregarding the quadratic component that does not contribute to $\Omega(k)$) is expressible as $H(k) = \mathbf{d}(k) \cdot \sigma$, the Berry curvature is defined as¹⁵

$$\Omega_{\mu\nu} = \frac{1}{2} \varepsilon_{\alpha\beta\gamma} \hat{d}_{\alpha}(k) \partial_{k_{\mu}} \hat{d}_{\beta}(k) \partial_{k_{\nu}} \hat{d}_{\gamma}(k), \quad (3)$$

where $\hat{\mathbf{d}}(k) = \frac{\mathbf{d}(k)}{d(k)}$. Applying this formalism in the case of Rashba Hamiltonian (Eq. 2), the $\Omega(k)$ takes the form:

$$\Omega(k) = \pm \frac{\alpha_R^2 \Delta}{2 \left[(\alpha_R k)^2 + \Delta^2 \right]^{3/2}} \hat{\mathbf{z}}. \quad (4)$$

In Eq. 4, $k^2 = k_x^2 + k_y^2$. The upper (lower) sign is for the spin-down (up) band. The Ω as a momentum-dependent magnetic field points out-of-plane (the z -axis). The $\Omega(k)$ vanishes as $\Delta \rightarrow 0$; the quenching of Δ (the Zeeman splitting) in this case restores *TRS* from which follows the relation, $\Omega(k) = 0$. A simple inspection of Eqs. 1 and 4 reveals that for a significant *ANE* a large $\Omega(k)$ is desirable which in turn requires a sizable Rashba splitting determined via the strength of the coefficient, α_R . The Rashba coefficient is strong in narrow band gap materials with considerable intrinsic *soc*, such as those belonging to the PbX family. The Rashba coupling coefficient is expressed as : $\alpha_R = \lambda_0 \langle F(z) \rangle$, where $\langle F(z) \rangle$ is the average out-of-plane (z -axis) electric field. The average value for $\langle F(z) \rangle$ is en/ϵ . Here, e is the electronic charge, the dopant density is n , and ϵ identifies the dielectric constant. The material-dependent λ_0 is given as¹⁶

$$\lambda_0 = \frac{\hbar^2}{2m^*} \frac{\Delta_{so}}{E_g} \frac{2E_g + \Delta_{so}}{(E_g + \Delta_{so})(3E_g + 2\Delta_{so})}. \quad (5)$$

For the specific case of PbX quantum wells, the parameters in Eq. 5 are defined at the L -valley; here, E_g is the direct band gap, the intrinsic *soc* is Δ_{so} , and m^* denotes the conduction band effective mass. The tuning of α_R is therefore, unlike, the intrinsic *soc* possible via changes to the band gap and effective mass in confined structures.

Before we carry out a quantitative analysis of the anomalous thermal behaviour, a set of remarks are in order: Firstly (1), the dielectric constant (dc) of PbTe is abnormally large (≈ 400), an outcome attributed to the high-polarizability of the chemical bond. This high dc ¹⁷ in addition to determining α_R via $\langle F(z) \rangle$ also couples with the low effective electron masses (in part, attributed to a substantial intrinsic *soc*) to set up a significant Bohr radius¹⁸ and thus enhancing carrier mobility. While thermoelectric applications require a pronounced mobility (and low thermal conductivity) for an optimized thermoelectric figure-of-merit (ZT), for the Rashba-driven *ANE*, a change in dc is reflected in α_R which clearly revises $\Omega(k)$ and consequently the thermal anomalous effects. The dc has been shown¹⁹ to be adjustable via simple lattice deformations of the rock salt crystal. In passing, it is useful to mention that polarizable *PbX* bonds also typically scupper the thermal conductivity to improve ZT . The second comment (2) pertains to additional *soc* terms that may occur in the Hamiltonian (Eq. 2). An extra *soc*-term (besides Rashba) for an in-plane electric field (F_{ip}) can be of the form $e\beta\hat{\sigma}\cdot(\mathbf{E}\times\mathbf{k})$. For an x -axis directed F_{ip} , the Hamiltonian receives a contribution expressed as $e\beta F_{ip}k_y\sigma_z$. The corresponding expression for $\Omega(k)$ by a direct application of the formula in Eq. 3 gives

$$\Omega(k) = \pm \frac{\alpha_R^2 (\Delta + e\beta F_{ip}k_y)}{2 \left[(\alpha_R k)^2 + (\Delta + e\beta F_{ip}k_y)^2 \right]^{3/2}} \hat{z}. \quad (6)$$

A more appealing situation emerges for an in-plane electric field solely directed along the y -axis; the *soc* in this case is simply $-e\beta F_{ip}k_x\sigma_z$ and manifestly counteracts Δ , the Zeeman splitting. For values of the y -directed F_{ip} such that $\Delta - e\beta F_{ip}k_x \rightarrow 0$, the out-of-plane (z -axis) magnetic field induced broken *TRS* is restored. The fulfillment of *TRS* to which we pointed out before leads to a ceasing of $\Omega(k)$ and the attendant *ANE*. It is therefore also apparent (from Eq. 6) that a union of the spin-orbit Hamiltonians through their respective coupling coefficients, α_R and β , allows a more detailed measure of control over the *ANE*-governed charge current (in a closed circuit). In fact, \mathcal{F}_{ip} can be considered applied from a gate terminal and serve as a threshold bias; for the correct polarity and magnitude, as $\Omega(k) \rightarrow 0$, it describes a complete turnoff setting unique to the material system. The final remark (3) considers the overall contribution of the two spin-split bands. Noting that $\Omega_{\downarrow}(k) = -\Omega_{\uparrow}(k)$, the complete *ANE* coefficient becomes $\mathcal{N}'_{ov} = ek_B / (4\pi^2\hbar) \int d^2k \Omega_{\downarrow}(k) [\mathcal{S}_{\downarrow}(k) - \mathcal{S}_{\uparrow}(k)]$. It is therefore straightforward to see that a spin-up band placed energetically above its spin-down counterpart when empty (or zero entropy) maximizes the *ANE*. Further, in connection to the spin-split bands and analogous to *ANE*, following Ref. 6, a spin Nernst coefficient (*SNE*) can be defined as

$$\mathcal{N}'_s = \frac{k_B}{2} \int \frac{d^2k}{4\pi^2} [\Omega_{\uparrow}(k) \mathcal{S}_{\uparrow}(k) - \Omega_{\downarrow}(k) \mathcal{S}_{\downarrow}(k)]. \quad (7)$$

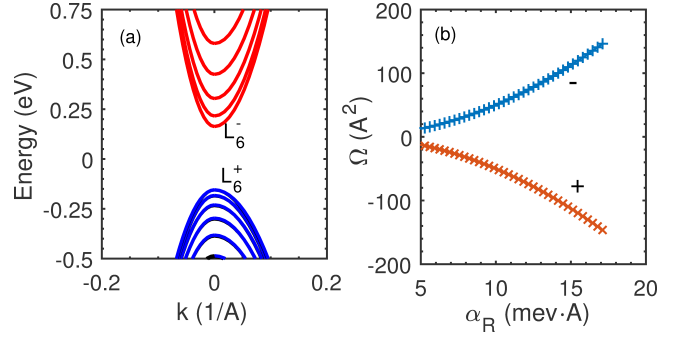


FIG. 2. The numerically obtained L -valley dispersion of a 6.0 nm wide [111] PbTe film along the high-symmetry path $\bar{K} - \bar{L} - \bar{\Gamma}$ is shown on the left panel (a). The right figure (b) plots (using Eq. 4) the Rashba-aided Berry curvature at the conduction band minimum ($|k|=0$) where the upper (lower) branch is for the spin-down (up) conduction state. The asymmetry-inducing electric field (out-of-plane) necessary for the Rashba splitting arises from an n -doping concentration; for purpose of numerical calculation, n was varied between $1 \times 10^{12} \text{ cm}^{-2}$ and $4 \times 10^{12} \text{ cm}^{-2}$. The dielectric constant of PbTe was set to 400 (see note below). The Zeeman splitting is treated as an external parameter and set to $\Delta = 2.0 \text{ meV}$ throughout.

It is, however, useful to reiterate that the $\Omega(k)$ in Ref. 6 strictly arises from the broken inversion symmetry of the monolayer transition metal dichalcogenide, unlike the Rashba-governed case here.

For numerical estimate of α_R , from which follows the $\Omega(k)$ and coefficients for *ANE* and *SNE*, a 6.0 nm wide PbTe film grown along the [111] axis is selected as the model structure. The L -valley band gap and effective mass (transverse) of this film from a $k.p$ calculation are $0.0565m_0$ and 0.33 eV . The free electron mass is $m_0 = 9.1 \times 10^{-31} \text{ kg}$. The dispersion of the 6.0 nm wide PbTe film and the accompanying Rashba-induced $\Omega(k)$ is shown in Fig. 2. Note that $\Omega(k)$ is plotted as a function of α_R , which is a function of material parameters and the film's Bloch conduction electrons effective mass. To proceed further a number of other parameters useful in determination of \mathcal{N}' and \mathcal{N}'_s must be defined: We begin by assigning the temperature (T) a pair of values: $T = \{125, 300\} \text{ K}$. The Fermi level is set to $E_f = 0.15 \text{ eV}$ from the bottom of the conduction band while the charge/dopant density is assumed to lie between 10^{12} cm^{-2} and $8 \times 10^{12} \text{ cm}^{-2}$. This dopant density furnished electric field lets α_R acquire values from $5.0 \text{ meV}\text{\AA} - 30.0 \text{ meV}\text{\AA}$. Inserting these numbers in Eqs. 1 and 7 and numerically integrating for $|k| \leq 0.3 \text{ 1/\AA}$, we plot \mathcal{N}' and \mathcal{N}'_s in Fig. 3 in units of ek_B/\hbar and $k_B/4\pi$, respectively. We only show the *ANE* coefficient for the spin-down band since the contribution of the spin-up band differs marginally from the former and carries a reversed sign. The closeness is simply a consequence of the moderate energy difference between the spin-split bands. Separately, the plot clearly reveals a more forceful display of *ANE* and *SNE* for weightier α_R , which expressly influences and enlarges $\Omega(k)$ - the engine behind anomalous effects. We make a note here

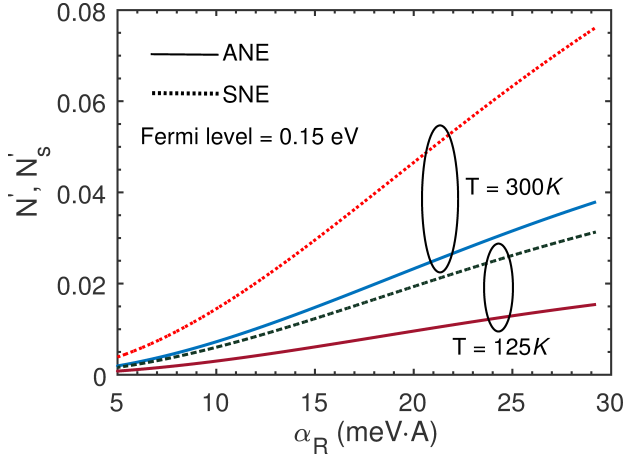


FIG. 3. The $ANE(\mathcal{N}')$ and $SNE(\mathcal{N}'_s)$ coefficients are plotted in units of ek_B/h and $k_B/4\pi$, respectively. The \mathcal{N}' is shown only for the spin-down band. Both coefficients increase as higher values of α_R are realized through doping or an external gate electrode. Additionally, at elevated temperatures that raise the entropy, larger coefficients are obtained. While the overall \mathcal{N}' taking both spin split bands into account nearly vanishes, the SNE allows the flow of a net spin current.

that the parameter α_R , in addition to dopant density changes is also amenable to further modification via adjustments to m^* , the band gap (E_g), and the intrinsic *soc*. While the *soc*, admittedly, is harder to modulate; however, m^* and E_g through varying degrees of confinement, layered-heterostructure design, and strain-like perturbation can substantially augment α_R . In line with schemes that may reinforce the anomalous thermal behaviour, it is also expedient to identify regions in momentum-space where $\Omega(k)$ and $\mathcal{S}(k)$ attain their highest values. The $\Omega(k)$ from Eq. 4 has a Lorentzian spread centered around the $|k| = 0$ point, which is the conduction band origin and reaches its maximum; likewise, the entropy has peaks on the Fermi surface and tails off away from it. For these two variables to amplify ANE and SNE , an intersecting region of momentum space must therefore be chosen to locate carriers with energy closely aligned to the Fermi surface while simultaneously ensuring that it isn't too far away from $|k| = 0$ for a reasonable $\Omega(k)$.

As a more definitive guide that ascertains the efficiency (η = output/input) of ANE , we can construct a paradigmatic Carnot engine like abstraction into which heat is pumped and ‘useful’ work extracted as power in a closed circuit. The power (‘output’) is $(\mathcal{N}'(-\nabla_x T))^2 \mathcal{R}$. The electric resistance of the closed circuit is \mathcal{R} . We consider a low temperature regime to ignore any phonon-driven thermal currents. A Carnot engine modeled on the NE must proceed by establishing a temperature gradient, where the desired heat current (‘input’) to maintain a temperature difference is given by the Fourier law: $J_Q = -\kappa \nabla_x T$. Here, κ is the thermal conductivity which is connected via the Wiedemann-Franz law (WFL) to its electric counterpart.²⁰ Briefly, the electric conductivity (for energy ε) using the linearized Boltzmann equation

is $\sigma = e^2 v_f^2 / 2 \int d\varepsilon D(\varepsilon) \tau(\varepsilon) (-\partial_\varepsilon f)$. The density-of-states, $D(\varepsilon)$, ignoring the linear Rashba and Zeeman term is $m^* / (\pi \hbar^2)$ and the Fermi velocity (v_f) is $\hbar k / m^*$. The scattering time is $\tau(\varepsilon)$. A direct application of WFL therefore gives the thermal conductivity as $\kappa = \mathcal{L} \sigma T$. Here, $\mathcal{L} = 2.44 \times 10^{-8} W \Omega K^{-2}$ is the Lorentz number. By following the outlined sequence of steps, the quantity η for the proposed Carnot engine is

$$\eta_{Carnot} = \frac{2\pi \hbar^2 [\mathcal{N}'^2 \nabla_x T] \mathcal{R}}{\mathcal{L} e^2 v_f^2 m^* \tau T}. \quad (8)$$

It is clearly noticeable from Eq. 8 that a low-effective mass improves efficiency - a result that ties well with the requirement of a strong Rashba coupled material, as both arise in compounds with a large intrinsic *soc*.

To summarize, we obtained analytic expressions for anomalous Nernst and spin Nernst coefficients tunable through the Rashba-created Berry curvature in PbTe films. Similarly, it is expected that narrow-gap and strongly spin-orbit coupled III-V materials such as InAs or InSb can give rise to comparable anomalous thermal currents. Besides, the SNE -origin anomalous spin current may find applications in spin caloritronics²¹ for a more diverse set of PbTe-like materials, rather than being limited, as it is hitherto, to mostly magnetic systems.

- ¹A. Abrikosov, *Fundamentals of the Theory of Metals* (Courier Dover Publications, 2017).
- ²D. Xiao, Y. Yao, Z. Fang, and Q. Niu, *Physical review letters* **97**, 026603 (2006).
- ³M. Gradhand, D. Fedorov, F. Pientka, P. Zahn, I. Mertig, and B. Györfy, *Journal of Physics: Condensed Matter* **24**, 213202 (2012).
- ⁴C. Zhang, S. Tewari, V. Yakovenko, and S. D. Sarma, *Physical Review B* **78**, 174508 (2008).
- ⁵X. Zhou, Y. Xu, and G. Jin, *Physical Review B* **92**, 235436 (2015).
- ⁶X. Yu, Z. Zhu, G. Su, and A.-P. Jauho, *Physical review letters* **115**, 246601 (2015).
- ⁷N. Averkiev, L. Golub, and M. Willander, *Journal of physics: condensed matter* **14**, R271 (2002).
- ⁸D. Xiao, G. Liu, W. Feng, X. Xu, and W. Yao, *Physical Review Letters* **108**, 196802 (2012).
- ⁹I. I. Ravich, *Semiconducting lead chalcogenides*, vol. 5 (Springer Science & Business Media, 2013).
- ¹⁰Z. Dughaish, *Physica B: Condensed Matter* **322**, 205 (2002).
- ¹¹Y. Xu, X. Zhou, and G. Jin, *Applied Physics Letters* **108**, 203104 (2016).
- ¹²J. Dimmock and G. Wright, *Physical Review* **135**, A821 (1964).
- ¹³I. Kang and F. W. Wise, *JOSA B* **14**, 1632 (1997).
- ¹⁴See accompanying note in Supplementary Material.
- ¹⁵S.-Q. Shen, *Topological insulators*, vol. 174 (Springer, 2012).
- ¹⁶E. e Silva, G. La Rocca, and F. Bassani, *Physical Review B* **55**, 16293 (1997).
- ¹⁷Y. Kanai and K. Shohno, *Japanese Journal of Applied Physics* **2**, 6 (1963).
- ¹⁸J. Heremans, R. Cava, and N. Samarth, *Nature Reviews Materials* **2**, 17049 (2017).
- ¹⁹H. Alves, A. Neto, L. Scolfaro, T. Myers, and P. Borges, *Physical Review B* **87**, 115204 (2013).
- ²⁰P. Sengupta, Y. Tan, G. Klimeck, and J. Shi, *Journal of Physics: Condensed Matter* **29**, 405701 (2017).
- ²¹G. Bauer, E. Saitoh, and B. J. Van Wees, *Nature materials* **11**, 391 (2012).